IEEE Access
Multidisciplinary | Rapid Review | Open Access Journal

Received April 2, 2019, accepted April 26, 2019, date of publication May 1, 2019, date of current version May 15, 2019.

Digital Object Identifier 10.1109/ACCESS.2019.2914267

High-Density Clutter Recognition and Suppression for Automotive Radar Systems

JUNGMIN YOON[1], (Student Member, IEEE), SEONGWOOK LEE[2], (Member, IEEE), SOHEE LIM[1], (Student Member, IEEE), AND SEONG-CHEOL KIM[1], (Senior Member, IEEE)

[1]Department of Electrical and Computer Engineering and Institute of New Media Communications (INMC), Seoul National University (SNU), Seoul 08826, South Korea

[2]Machine Learning Lab, AI & SW Research Center, Samsung Advanced Institute of Technology (SAIT), Suwon 16678, South Korea

Corresponding author: Seong-Cheol Kim (sckim@maxwell.snu.ac.kr)

ABSTRACT In this paper, an enhanced high-density clutter recognition and suppression method for automotive frequency-modulated continuous wave (FMCW) radar systems are presented. In a high-density clutter environment, such as guardrails, tunnels, and soundproof walls, the target detection performance is degraded because many undesired beat frequency components are detected due to a large number of reflectors in road structures. Thus, we propose to recognize and suppress the high-density clutter to enhance the target detection performance. On the basis of the distinctive beat frequency distribution in the high-density clutter environment, we propose a recognition parameter. After clutter recognition, we suppress the clutter using the correlation between up-chirp and down-chirp received signals. By using the experimental results obtained from various road environments, we applied our proposed recognition and suppression method and verified its performance. As a result, the high-density clutter was clearly recognized and effectively suppressed by the proposed method. In addition, more accurate and reliable target detection can be achieved when the clutter-suppressed signal is used, which can ensure the safety of drivers using automotive FMCW radars.

INDEX TERMS Automotive radar, clutter recognition and suppression, frequency-modulated continuous wave (FMCW).

I. INTRODUCTION

Recently, an extensive interest has been focused on autonomous driving vehicles [1]. For autonomous driving, vehicles must recognize the surrounding road environment and determine the driving direction by themselves. To recognize the driving environments, various automotive devices are being used. For example, camera and lidar sensors are typical devices that use light to recognize road environments [2]–[4]; however, the performance of these sensors cannot be fully guaranteed under harsh weather conditions such as heavy rains and thick fog. These problems can be overcome using radar sensors that are robust to bad weather conditions [5]. Therefore, the use of radar sensors that recognize the driving environments has become more attractive.

For automotive radars, frequency-modulated continuous wave (FMCW) radars using the millimeter-wave frequency band are widely used due to their low production costs and low power consumption [6]. These FMCW radars extract the target information (e.g., relative velocity and relative distance) from the received radio wave signals. When a radar-equipped vehicle drives in road environments with reflectors, undesired signals are received [7], [8]. These undesired signals are called clutter. Some studies were conducted to recognize the clutter signals from specific road structures such as guardrails and bridges in [9]–[11]. Unfortunately, there are many types of structures on roads. Some road structures such as tunnels and soundproof walls generate a large number of high-intensity clutter signals. In a high-density clutter environment, which includes a large number of high-intensity clutter signals, the intensity of a signal reflected from the desired target may be weaker than that of the clutter, or the clutter may be recognized as a signal reflected from a desired target [8], [12]. In this situation, the malfunction probability of autonomous emergency braking (AEB) also increases by high-density clutter signals.

The associate editor coordinating the review of this manuscript and approving it for publication was Weimin Huang.

In such a case, a method that can overcome the misdetection of the desired target due to high-density clutter is required.

To suppress the high-density clutter, a clutter recognition method should first be developed. Nevertheless, studies on high-density clutter environment recognition using automotive radar sensors have not been intensively conducted. In general, in a radar system using slow-chirp signals, pairing between up-chirp and down-chirp received signals is required to determine the relative distance and the relative velocity between the radar-equipped vehicle and the target [13]. This is the same for clutter signals. To suppress the clutter signals, we have to find the stationary targets by pairing. However, it is difficult to pair individual reflected signals in a high-density clutter environment where there are many high-intensity clutter signals caused by large artificial road structures. In [7], [8], a method that only recognized iron tunnels by applying the concept of Shannon entropy (SE) [14] to the frequency-domain received signals was proposed. In addition, the authors in [12] recognized road structures with periodic steel frames, in addition to the iron tunnels, by identifying the fundamental frequency and its harmonics in the frequency-domain received signal. Although this method effectively recognized the structures that generated high-density clutter, it could only be applied to periodic structures. After the recognition of the high-density clutter environment, the clutter must also be suppressed to enhance the target detection performance. In [12], [15], the authors proposed to suppress the clutter by eliminating the fundamental frequency components and their harmonics from the frequency-domain received signals; however, because these suppression methods can only be used in periodically installed structures, a clutter suppression method that can be used in more general driving environments is needed. In [16], [17], the authors suppressed the clutter using the correlation between chirp signals; however, the recognition of high-density clutter environments was not discussed.

Therefore, we propose a high-density clutter recognition and suppression method that can be used in general conditions regardless of the periodicity of road structures. On the basis of the fact that the beat frequency distribution in a high-density clutter environment is different from that in a normal road environment, we define a recognition parameter. In addition, we suppress the clutter using the correlation between the up-chirp and down-chirp received signals. Because reflectors that compose the road structure are stationary, the Doppler frequencies of the reflected signals have the same value [18]. On the other hand, the Doppler shift caused by the velocity of the desired target has different values for each target. Thus, if the correlation between the up-chirp and down-chirp received signals is considered, the Doppler frequency caused by the clutter can be extracted. Then, by shifting the down-chirp signal using the extracted frequency shift and subtracting it from the up-chirp signal, the clutter can be suppressed while maintaining the signals reflected from the desired targets. By using the measurement results obtained from various road environments, we applied our proposed recognition and suppression method and verified its performance. Our method showed more stable and reliable recognition result than that of the method in [8]. In addition, if the clutter is suppressed by our proposed method, target detection can be properly performed using the constant false alarm rate (CFAR) algorithm, and the probability of an AEB malfunction can be reduced [19].

The rest of this paper is organized as follows. In Section II, the fundamentals of an automotive FMCW radar system and the received signal analysis in the frequency domain are introduced. The proposed high-density clutter recognition method is presented in Section III. Then, clutter suppression is explained in Section IV. In Sections III and IV, the performance of the proposed method is verified by applying it to actual measurement results. Finally, we conclude the paper in Section V.

II. FREQUENCY-DOMAIN ANALYSIS IN AUTOMOTIVE FMCW RADAR SYSTEM

A. FUNDAMENTALS OF AUTOMOTIVE FMCW RADAR SYSTEM

In this section, we describe the transmission and reception of signals in an automotive FMCW radar system. In this study, one period of the transmitted FMCW signal is defined as a scan. One scan consists of the transmission time of a chirp signal and the signal processing time. The frequency of the chirp signal linearly increases and decreases according to time [20]. A signal with increasing frequency is called an up-chirp signal, and a signal with decreasing frequency is called a down-chirp signal. We let $s^U(t)$ and $s^D(t)$ be the up-chirp and down-chirp transmitted signals, respectively. These are expressed as

$$\begin{aligned} s^U(t) &= A\cos\left(2\pi(f_c - \frac{W}{2})t + \pi\frac{W}{T_P}t^2\right), \\ s^D(t) &= A\cos\left(2\pi(f_c + \frac{W}{2})t - \pi\frac{W}{T_P}t^2\right), \end{aligned} \tag{1}$$

where A, f_c, W, and T_P denote the amplitude, carrier frequency, operating bandwidth, and sweep time for both chirp signals, respectively. Then, transmitted signal $s(t)$ in one scan is expressed as follows:

$$s(t) = \begin{cases} s^U(t) & (0 \le t < T_P) \\ s^D(t - T_P) & (T_P \le t < 2T_P) \\ 0 & (2T_P \le t < T_S) \end{cases}, \tag{2}$$

where T_S denote the period of one scan. This transmitted signal is reflected by multiple targets in the field of view of the radar systems. The signal reflected from the l-th target is received with propagation time delay t_{d_l}, which is expressed as

$$r_l(t) = \begin{cases} r_l^U(t) & (t_{d_l} \le t < T_P + t_{d_l}) \\ r_l^D(t - T_P) & (T_P + t_{d_l} \le t \le 2T_P + t_{d_l}) \\ 0 & (2T_P + t_{d_l} \le t < T_S + t_{d_l}) \end{cases}, \tag{3}$$

where $l\,(l = 1, 2, \cdots, L)$ is the index of each target and L is the total number of targets. In (3), $r_l^U(t)$ and $r_l^D(t)$ are the received signals corresponding to the up-chirp and down-chirp transmitted signals, which are given by

$$\begin{aligned} r_l^U(t) &= A_{R_l} \cos\left(2\pi(f_c + f_{d_l} - \frac{W}{2})(t - t_{d_l}) + \pi \frac{W}{T_P}(t - t_{d_l})^2\right), \\ r_l^D(t) &= A_{R_l} \cos\left(2\pi(f_c + f_{d_l} + \frac{W}{2})(t - t_{d_l}) - \pi \frac{W}{T_P}(t - t_{d_l})^2\right). \end{aligned} \tag{4}$$

Each $r_l(t)$ reflected from different L targets has different amplitude A_{R_l}, Doppler frequency f_{d_l}, and time delay t_{d_l}. In addition, f_{d_l} and t_{d_l} are caused by the relative velocity and relative distance between the radar-equipped vehicle and l-th target. At the receiver, the total received signal is composed of the signals reflected from multiple targets, which is expressed as

$$r(t) = \sum_{l=1}^{L} r_l(t) \quad (t_d^{max} \le t < T_S), \tag{5}$$

where t_d^{max} is $\max_{l\in\{1,2,\cdots,L\}} t_{d_l}$.

After the signal reception, $r(t)$ passes through the frequency mixer. In the frequency mixer, $r(t)$ is multiplied by $s(t)$, and baseband signal $x(t)$ is extracted by low-pass filtering multiplied signal $r(t)s(t)$, which is expressed as

$$\begin{aligned} x(t) &= LPF\,(r(t)s(t)) \\ &= \begin{cases} x^U(t) & (t_d^{max} \le t < T_P) \\ x^D(t - T_P) & (T_P + t_d^{max} \le t \le 2T_P), \end{cases} \end{aligned} \tag{6}$$

where

$$\begin{aligned} x^U(t) &= \frac{A}{2}\sum_{l=1}^{L} A_{R_l} \cos\left(2\pi(\frac{W}{T_P}t_{d_l} - f_{d_l})t \right. \\ &\quad \left. + 2\pi(f_c + f_{d_l} - \frac{W}{2})t_{d_l} - \pi\frac{W}{T_P}t_{d_l}^2\right) + n(t), \\ x^D(t) &= \frac{A}{2}\sum_{l=1}^{L} A_{R_l} \cos\left(2\pi(\frac{W}{T_P}t_{d_l} + f_{d_l})t \right. \\ &\quad \left. - 2\pi(f_c + f_{d_l} + \frac{W}{2})t_{d_l} - \pi\frac{W}{T_P}t_{d_l}^2\right) + n(t). \end{aligned} \tag{7}$$

In (6), $LPF(\cdot)$ denotes the low-pass filter output, and $n(t)$ is the noise signal added to the low-pass filter output. Baseband signals $x^U(t)$ and $x^D(t)$ are composed of L cosine wave signals with constant frequency components. These frequency components, which are called beat frequencies, contain information of each target, such as the relative velocity and relative distance. If we denote $f_{b_l}^U$ and $f_{b_l}^D$ as the beat frequencies that can be extracted from $x^U(t)$ and $x^D(t - T_P)$ for the l-th target, the relationship between $f_{b_l}^U$ and $f_{b_l}^D$ is respectively expressed by the following equations:

$$\begin{aligned} f_{b_l}^U &= \frac{W}{T_P}t_{d_l} - f_{d_l} \\ &= \frac{W}{T_P}\frac{2R_l}{v_c} - \frac{2v_l}{v_c}f_c \quad (t_d^{max} \le t < T_P), \\ f_{b_l}^D &= \frac{W}{T_P}t_{d_l} + f_{d_l} \\ &= \frac{W}{T_P}\frac{2R_l}{v_c} + \frac{2v_l}{v_c}f_c \quad (T_P + t_d^{max} \le t \le 2T_P), \end{aligned} \tag{8}$$

where v_c, v_l, and R_l denote the speed of the radar signal, relative velocity between the radar-equipped vehicle and l-th target, and relative distance between the radar-equipped vehicle and l-th target, respectively. Thus, by extracting the beat frequencies in both chirp signals and pairing them, we can estimate v_l and R_l of each target [19].

B. RECEIVED SIGNAL ANALYSIS IN THE FREQUENCY DOMAIN

In general, many beat frequency components exist in each scan. Those beat frequency components can be extracted by applying fast Fourier transform (FFT) to $x^U(t)$ and $x^D(t)$. We let $x_p^U[n]$ and $x_p^D[n]$ be sampled $x^U(t)$ and $x^D(t)$ in the p-th scan with sampling frequency f_s. Then, $x_p^U[n]$ and $x_p^D[n]$ are converted to frequency-domain signals $\mathbf{X}_p^U$ and $\mathbf{X}_p^D$ using the FFT, which are expressed as

$$\begin{aligned} \mathbf{X}_p^U &= \left[X_p^U[0],\, X_p^U[1],\, \cdots,\, X_p^U[\frac{N_F}{2} - 1]\right], \\ \mathbf{X}_p^D &= \left[X_p^D[0],\, X_p^D[1],\, \cdots,\, X_p^D[\frac{N_F}{2} - 1]\right], \end{aligned} \tag{9}$$

where $X_p^U[k]$ and $X_p^D[k]\,(k = 0, 1, \cdots, \frac{N_F}{2} - 1)$ denote the k-th frequency components of the FFT output and N_F is the number of FFT points. Because the FFT output is symmetrical around $\frac{N_F}{2}$, the frequency components from $\frac{N_F}{2}$ to $N_F - 1$ are not considered. In addition, the absolute values of each element in $\mathbf{X}_p^U$ and $\mathbf{X}_p^D$ are used to effectively show the magnitudes of the frequency components, which are respectively expressed as

$$\begin{aligned} \lceil \mathbf{X}_p^U \rceil_{||} &= \left[|X_p^U[0]|,\, |X_p^U[1]|,\, \cdots,\, |X_p^U[\frac{N_F}{2} - 1]|\right], \\ \lceil \mathbf{X}_p^D \rceil_{||} &= \left[|X_p^D[0]|,\, |X_p^D[1]|,\, \cdots,\, |X_p^D[\frac{N_F}{2} - 1]|\right], \end{aligned} \tag{10}$$

where $\lceil\cdot\rceil_{||}$ is a notation that considers the absolute values of all elements in the vector.

III. PROPOSED HIGH-DENSITY CLUTTER RECOGNITION METHOD

A. EXPERIMENTS IN ROAD ENVIRONMENTS

In this section, we first introduce the adverse effect of high-density clutter using the experimental results. Then, we derive a method that can recognize high-density clutter road environments by analyzing the measurement results. The specifications of our radar system used in the measurements are listed in Table 1. We used long-range radar (LRR), which

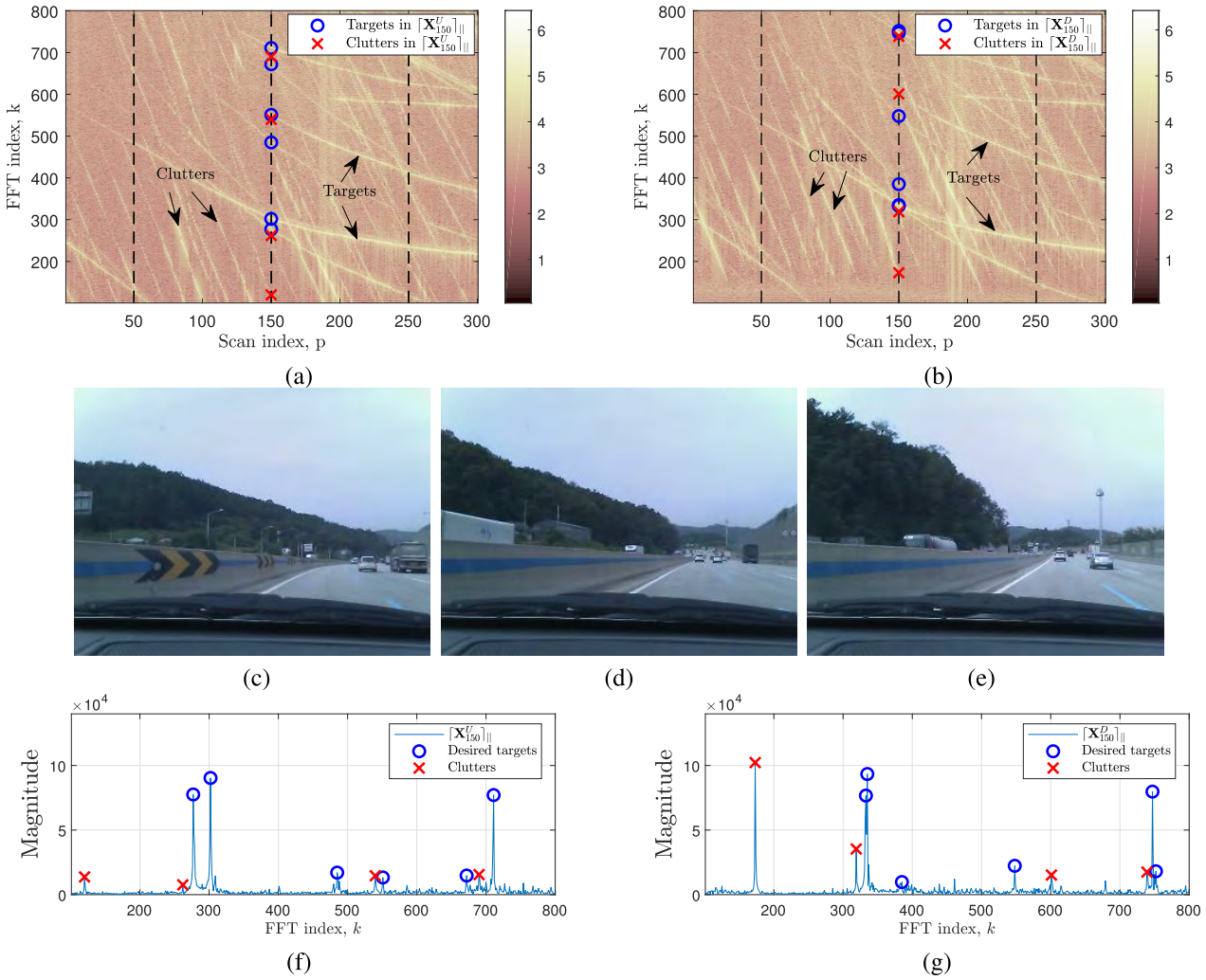

FIGURE 1. (a) Accumulated $\lceil \mathbf{X}^U_p \rceil_{||}$. (b) Accumulated $\lceil \mathbf{X}^D_p \rceil_{||}$. (c) Snapshot for $p = 50$. (d) Snapshot for $p = 150$. (e) Snapshot for $p = 250$. (f) $\lceil \mathbf{X}^U_{150} \rceil_{||}$. (g) $\lceil \mathbf{X}^D_{150} \rceil_{||}$.

TABLE 1. Measurement system.

Radar type	Long-range radar
Field of view (FoV)	$-10°$ to $10°$, azimuth
Receiving antenna type	Uniform linear array
Number of array elements	4
Antenna spacing	1.8λ
Modulation scheme	FMCW
Carrier frequency, f_c	76.5 GHz
Bandwidth, W	500 MHz
Sweep time, T_P	5 ms
Signal transmission time, $2T_P$	10 ms
Signal processing time	50 ms
One period of a scan, T_S	60 ms
Number of FFT points, N_F	2048
Sampling frequency, f_s	390.625 kHz
Max. detection distance, $\frac{T_P f_s}{4W} v_c$	292.9688 m

is mainly used for adaptive cruise control (ACC) and AEB in high-speed driving environments [21]. The antenna is implemented with 1.8 λ of antenna spacing to secure the angular resolution within the FoV. In the experiment, the maximum speed of the vehicle was 110 km/h.

In our measurement, more than 300 scans were captured for each test environment. For example, the measurement result in a normal road environment is shown in Fig. 1. Figs. 1 (a) and (b) show the accumulated $\lceil \mathbf{X}^U_p \rceil_{||}$ and $\lceil \mathbf{X}^D_p \rceil_{||}$ from 300 scans. In addition, Figs. 1 (c), (d), and (e) show snapshots of the 50-th ($p = 50$), 150-th ($p = 150$), and 250-th ($p = 250$) scans, and Figs. 1 (f) and (g) show $\lceil \mathbf{X}^U_{150} \rceil_{||}$ and $\lceil \mathbf{X}^D_{150} \rceil_{||}$. In Figs. 1 (a) and (b), we can see that a trajectories of several target and clutter signals are distributed in accumulated $\lceil \mathbf{X}^U_p \rceil_{||}$ and $\lceil \mathbf{X}^D_p \rceil_{||}$. $f^U_{b_l}$ and $f^D_{b_l}$ of the targets and the clutter signals located in the field of view (FoV) show higher magnitudes compared with those of the other frequency components. The trajectories of the target signals are gently tilted, while the trajectories of the clutter signals are tilted at a high slope. This is because the distance between the stationary object and the vehicle changes rapidly. In this figure, the clutter signals are rarely distributed. In this environment, a radar-equipped vehicle can detect the desired

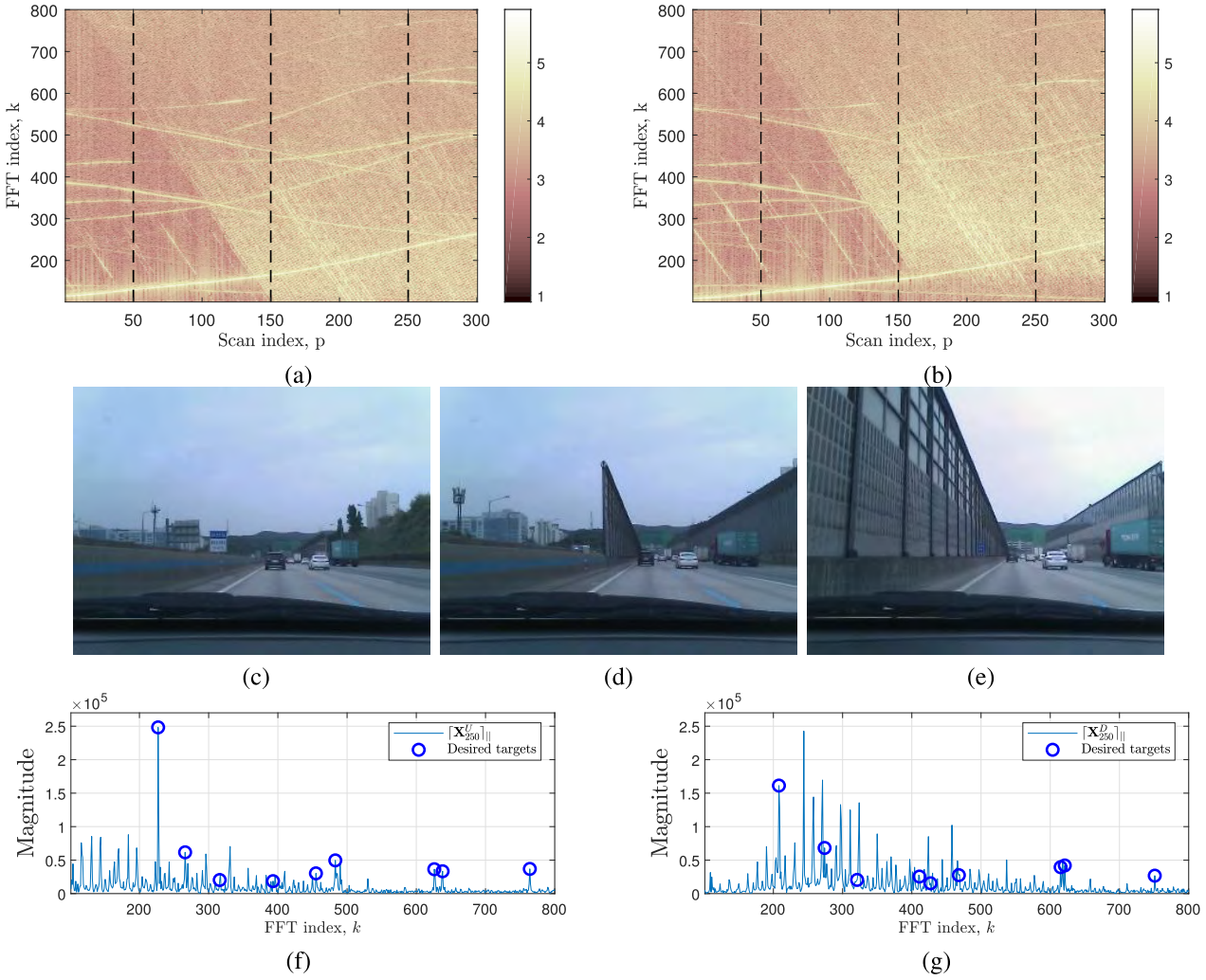

FIGURE 2. (a) Accumulated $\lceil \mathbf{X}_p^U \rceil_{||}$. (b) Accumulated $\lceil \mathbf{X}_p^D \rceil_{||}$. (c) Snapshot for $p = 50$. (d) Snapshot for $p = 150$. (e) Snapshot for $p = 250$. (f) $\lceil \mathbf{X}_{250}^U \rceil_{||}$. (g) $\lceil \mathbf{X}_{250}^D \rceil_{||}$.

target and extract its relative distance and velocity by pairing $f_{b_l}^U$ and $f_{b_l}^D$.

On the other hand, Figs. 2 and 3 show the measurement results in two different road environments with high-density clutter. For the case shown in Fig. 2 (i.e., Scenario A), the radar-equipped vehicle drives in a normal road environment at first. After a certain period of time has passed, the radar-equipped vehicle enters a road surrounded by iron soundproof walls, as shown in Fig. 2 (d). In this case, Figs. 2 (f) and (g) show that a number of unwanted frequency components corresponding to signals reflected from the soundproof walls appear. We define these unwanted frequency components as clutter in this study. When high-density clutter exists, the signal reflected from the desired target cannot be identified because its beat frequency is buried by the clutter, as shown in Figs. 2 (f) and (g). Fig. 3 shows another measurement result obtained in a high-density clutter environment such as a tunnel environment (i.e., Scenario B). Figs. 3 (c), (d), and (e) show snapshots for $p = 50,\ 150,\ 250$ when the radar-equipped vehicle passes a tunnel. When the radar-equipped vehicle drives into the tunnel, the beat frequency corresponding to the desired target cannot be detected by the clutter, as shown in Figs. 3 (f) and (g). This high-density clutter signals in $\lceil \mathbf{X}_p^U \rceil_{||}$ appears in the same form for the various values of T_P, T_S, and N_F. For example, if T_P, T_S, and N_F increase to twice their values, the maximum target detection distance also increases, the frequency of the target detection process is reduced by half, and the detection distance resolution remains the same. Regardless of this change, the signal corresponding to high-density clutter is still received, and it appears in the form of reflected waves owing to a large number of stationary reflectors as in the accumulated $\lceil \mathbf{X}_p^U \rceil_{||}$ of Figs. 2 and 3.

When the radar-equipped vehicle drives in a normal road environment, the signal reflected from the desired target is received by our radar system because no other strong reflectors exist. In this environment, the conventional beat frequency estimation algorithm can detect the beat frequency of targets without performance degradation, i.e., the magnitude of the desired target is higher than the threshold of the

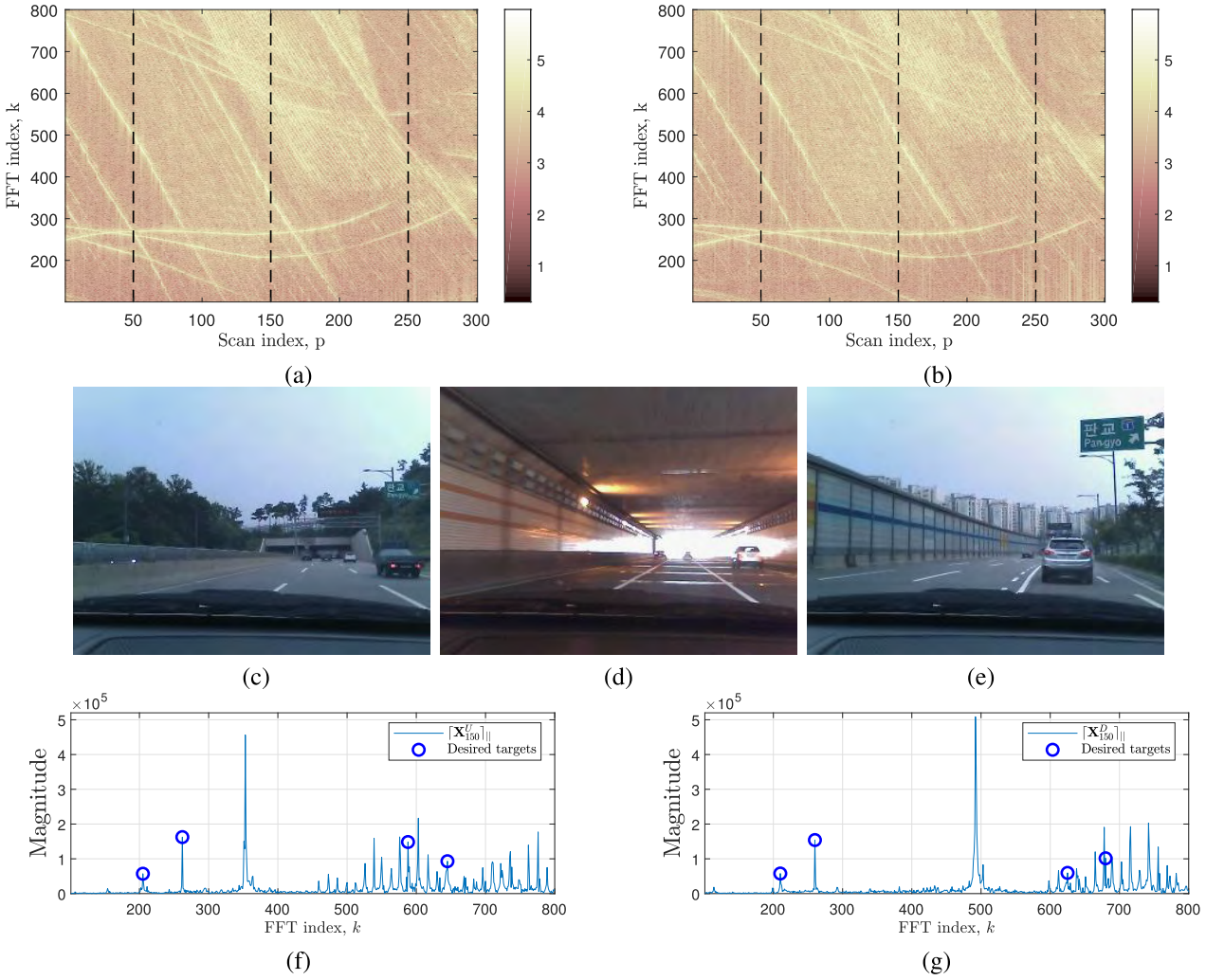

FIGURE 3. (a) Accumulated $\lceil \mathbf{X}_p^U \rceil_{||}$. (b) Accumulated $\lceil \mathbf{X}_p^D \rceil_{||}$. (c) Snapshot for $p = 50$. (d) Snapshot for $p = 150$. (e) Snapshot for $p = 250$. (f) $\lceil \mathbf{X}_{150}^U \rceil_{||}$. (g) $\lceil \mathbf{X}_{150}^D \rceil_{||}$.

CFAR algorithm [19]. However, when many reflectors exist in road environments such as guardrails, soundproof walls, and tunnels, the clutter density increases. In the latter case, target detection using the CFAR algorithm cannot operate properly [22]. Thus, a method to recognize the road environments with high-density clutter and to suppress its adverse effects on target estimation is required.

B. HIGH-DENSITY CLUTTER RECOGNITION METHOD

When the radar-equipped vehicle drives through normal roads as shown in Figs. 1, the high-intensity elements in $\lceil \mathbf{X}_p^U \rceil_{||}$ mainly comes from desired targets within the limited FoV and detection range. The number of high-intensity elements is limited to a relatively small number compared to N_F. The intensity of the remaining element is low enough to be distinguishable from these few high-intensity elements. However, when the radar-equipped vehicle travels through high-density clutter environments, significantly large numbers of high-intensity elements appear as shown in Figs. 2 and 3. Although the low-intensity elements still accounts for the largest portion in high-density clutter environments, the occupancy of high-intensity elements among all $|X_p^U[k]|$ appears at a level that distinguishes whether the driving environment is normal or high-density clutter environments.

To observe this difference of high-intensity elements occupancy, we sort all $|X_p^U[k]|$ in descending order, and compare the sorted $|X_p^U[k]|$, named $\mathbf{Y}_p^U$, of normal and high-density clutter environments. Fig. 4 (a) shows ordered element-wise averaged results of one hundred normalized-$\mathbf{Y}_p^U$, and Fig. 4 (b) shows element-wise ratio of the two results in Fig. 4 (a). Results were evaluated in normal and high-density clutter environments. Received signals in 1-st to 100-th scans of Fig. 1 (f) and 201-st to 300-th scans of Fig. 2 (a) were used as $\mathbf{Y}_p^U$ for the normal and high-density clutter environments, respectively. The x-axis represents the index of $\mathbf{Y}_p^U$, and it is log-scaled for visibility. We observed the results divided into three sets with elements of N_1, N_2, and N_3. The first set $\mathbf{Y}_p^{U_1}$

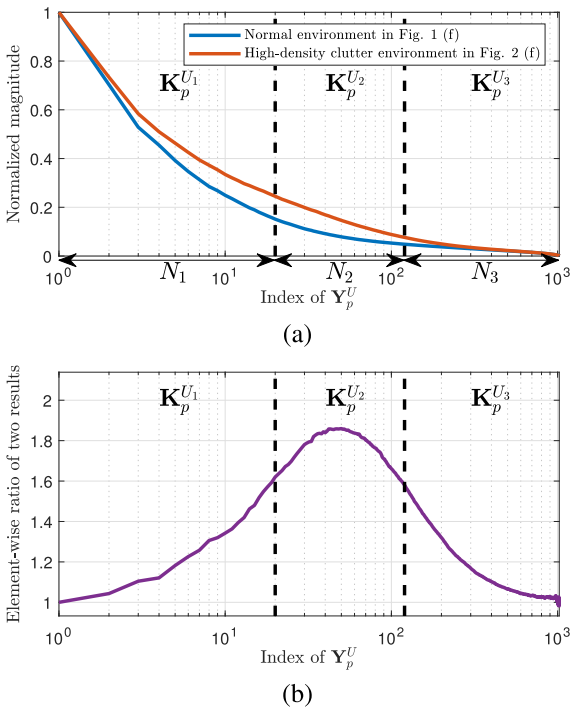

FIGURE 4. (a) Element-wise averaged normalized-$\mathbf{Y}_p^U$ in two different road environments. (b) Element-wise ratio of two results in (a).

consist of the first N_1 elements of $\mathbf{Y}_p^U$. N_1 is a small number considering the maximum number of targets within the limited FoV and detection range. When the radar-equipped vehicle drives through the normal road, elements of the first set consist of a few highest-intensity elements that are likely to have been received from desired targets. In the case of a high-density clutter environment, elements of the first set still consist of high-intensity elements received from desired targets or artificial road structures. Whether the radar-equipped vehicle travels through a normal road or a high-density clutter environment, the first set is usually filled with high-intensity elements. As a result, the elements of the first set have similar magnitude level in both environments as shown in Figs. 4 (a) and (b). The second set $\mathbf{Y}_p^{U_2}$ consist of the next N_2 elements of $\mathbf{Y}_p^U$. Elements of the third set $\mathbf{Y}_p^{U_3}$ are the last N_3 elements ($N_1 + N_2 + N_3 = \frac{N_F}{2}$). N_2 is several times larger value of N_1 but several times smaller than N_3; $N_1 \ll N_2 \ll N_3$. These two sets consist of a large number of noisy elements with low-intensity in the normal road environment. However, if the radar-equipped vehicle passes through high-density clutter environment, the second set is filled with elements that are likely to be high-intensity clutter signals, while the elements of the third set are still noisy elements. Consequently, $\mathbf{Y}_p^{U_2}$ shows largest difference as shown in Fig. 4 (b). On this basis, we can define the first recognition parameter for the high-density clutter environment as

$$\alpha_p = \frac{\frac{1}{N_2}\sum_{k\in\mathbf{K}_p^{U_2}} |X_p^U[k]|}{\frac{1}{N_1}\sum_{k\in\mathbf{K}_p^{U_1}} |X_p^U[k]|}, \tag{11}$$

where $\mathbf{K}_p^{U_1}$, $\mathbf{K}_p^{U_2}$, and $\mathbf{K}_p^{U_3}$ are the FFT index sets of the elements in each set, respectively. α_p can also be calculated using $\lceil \mathbf{X}_p^D \rceil_{||}$. However, calculating α_p with a down-chirp signal is similar to calculating α_p with an up-chirp signal because the distribution of $\lceil \mathbf{X}_p^U \rceil_{||}$ is similar to that of $2f_{d_l}$-shifted $\lceil \mathbf{X}_p^D \rceil_{||}$.

In (11), α_p is calculated by using only up-chirp received signal $x_p^U[n]$. In addition to $x_p^U[n]$, the down-chirp received signal $x_p^D[n]$ can also be used for high-density clutter environment recognition. To utilize the down-chirp received signal, we first investigate the relationship between the beat frequencies extracted from both chirp signals for the l-th target. The relationship between $f_{b_l}^U$ and $f_{b_l}^D$ in (8) for the l-th target is expressed as

$$f_{b_l}^U = f_{b_l}^D - 2f_{d_l}. \tag{12}$$

In addition, the beat frequencies in the high-density clutter environment have a similar relationship to (12). If we denote m ($m = 1, 2, \cdots, M$) as the index of the reflector that generates high-density clutter, the relationship between the beat frequencies extracted from both received chirp signals is expressed as

$$f_{b_m}^U = f_{b_m}^D - 2f_{d_m}, \tag{13}$$

where $f_{d_m} = \frac{2v_{d_m}}{v_c} f_c$ is the Doppler frequency caused by the relative velocity v_{d_m} between the radar-equipped vehicle and m-th reflector. Because reflectors are stationary objects, v_{d_m} for all m is equal to the velocity of the radar-equipped vehicle [18]. Accordingly, f_{d_m} also has the same values for all m. Thus, (13) can also be expressed as

$$f_{b_m}^U = f_{b_m}^D - 2f_e = f_{b_m}^D - \frac{2v_e}{v_c} f_c, \tag{14}$$

where f_e and v_e are the Doppler frequency and relative velocity, respectively, with constant values for all m. The magnitudes of the beat frequencies for the same object have almost similar values in both chirp signals. Because the length of a road structure is a few dozen of meters in scale, it has a relatively long length compared to the distance that can be traveled by the radar-equipped vehicle in T_P. As a result, clutter signals having a strong signal intensity, which come from stationary objects during the period of the up-chirp received signal, arrive with the same intensity in the period of the down-chirp received signal. Thus, the relationship between $|X_p^U[k]|$ and $|X_p^D[k]|$ for the l-th target and m-th reflector can be respectively expressed as

$$|X_p^U[k_{b_l}^U]| \cong |X_p^D[k_{b_l}^D]| = |X_p^D[k_{b_l}^U + 2k_{d_l}]|, \tag{15}$$

and

$$|X_p^U[k_{b_m}^U]| \cong |X_p^D[k_{b_m}^D]| = |X_p^D[k_{b_m}^U + 2k_e]|, \tag{16}$$

where $k_{b_l}^U$, $k_{b_l}^D$, k_{d_l}, $k_{b_m}^U$, $k_{b_m}^D$, and k_e correspond to the frequency-domain indices of $f_{b_l}^U$, $f_{b_l}^D$, f_{d_l}, $f_{b_m}^U$, $f_{b_m}^D$, and f_e, respectively. In (15) and (16), $|X_p^U[k_{b_l}^U]|$ and $|X_p^U[k_{b_m}^U]|$ have similar relationships; however, frequency shifts $2k_{d_l}$

and $2k_e$ are different for the desired targets and reflectors. As expressed in (16), the amount of frequency shift between $|X_p^U[k]|$ and $|X_p^D[k]|$ is the same as $2k_e$ for all M reflectors, but it is not the same for all L targets [18]. In addition, the number of reflectors is larger than that of the desired targets in the high-density clutter environment (i.e., $M \gg L$). Thus, we expect that the correlation between $\lceil \mathbf{X}_p^U \rceil_{||}$ and $\lceil \mathbf{X}_p^D \rceil_{||}$ is high in a high-density clutter environment. Consequently, k_e can be estimated using the correlation between $\lceil \mathbf{X}_p^U \rceil_{||}$ and $\lceil \mathbf{X}_p^D \rceil_{||}$, which is expressed as

$$2\widetilde{k}_e = \underset{q\in\{0,1,\cdots,2k_e^{MAX}\}}{\operatorname{argmax}} \sum_{k=0}^{\frac{N_F}{2}-1} |X_p^U[k]||X_p^D[k+q]|, \quad (17)$$

where k_e^{MAX} can be limited according to the maximum speed of the radar-equipped vehicle. In addition, $|X_p^D[k+q]|$ with index $k+q > \frac{N_F}{2}-1$ is regarded as zero in (17). Using this estimated frequency shift, the effect of the high-density clutter can be suppressed from $\lceil \mathbf{X}_p^U \rceil_{||}$ by subtracting $|X_p^D[k+2\widetilde{k}_e]|$ from $|X_p^U[k]|$. However, the elements that correspond to $f_{b_l}^D$ of $|X_p^D[k]|$ can appear as negative values with large magnitudes in $|X_p^U[k]|-|X_p^D[k+2\widetilde{k}_e]|$. These negative values, which are not caused by the clutter signals, should be eliminated. To avoid the appearance of these unwanted components, we set the negative values in $|X_p^U[k]|-|X_p^D[k+2\widetilde{k}_e]|$ to zero:

$$|\widetilde{X}_p^U[k]| = \lceil |X_p^U[k]| - |X_p^D[k+2\widetilde{k}_e]| \rceil_+, \quad (18)$$

where $\lceil \cdot \rceil_+$ represents a notation that makes the output zero for a negative input value. Through this process, the beat frequencies of the desired targets remain in $|\widetilde{X}_p^U[k]|$. Then, by subtracting $|\widetilde{X}_p^U[k]|$ from $|X_p^U[k]|$, the beat frequencies in the high-density clutter environment can be extracted. According to this argument, we can define the second high-density clutter recognition parameter as

$$\beta_p = \frac{\sum_{k=0}^{\frac{N_F}{2}-1} \left(|X_p^U[k]|^2 - |\widetilde{X}_p^U[k]|^2 \right)}{\sum_{k=0}^{\frac{N_F}{2}-1} |X_p^U[k]|^2}. \quad (19)$$

This parameter is highly dependent on the effect of the clutter. In high-density clutter environments, it has a high value because of the number of beat frequencies; otherwise, it has a small value in normal road environments.

To further improve (17), we only consider the first and second sets of up- and down-chirp signals for the frequency shift estimation because no large difference exists in the third set among the differing road environments. Let $\mathbf{Y}_p^{D_1}$, $\mathbf{Y}_p^{D_2}$, and $\mathbf{Y}_p^{D_3}$ be the classified signal sets for down-chirp signals with the same manner for the signal sets of up-chirp signals, $\mathbf{Y}_p^{U_1}$, $\mathbf{Y}_p^{U_2}$, and $\mathbf{Y}_p^{U_3}$, respectively. Then, $\mathbf{K}_p^{D_1}$, $\mathbf{K}_p^{D_2}$, and $\mathbf{K}_p^{D_3}$ are the FFT index sets of $\mathbf{Y}_p^{D_1}$, $\mathbf{Y}_p^{D_2}$, and $\mathbf{Y}_p^{D_3}$, respectively. Thus, we reconstruct $\lceil \mathbf{X}_p^U \rceil_{||}$ and $\lceil \mathbf{X}_p^D \rceil_{||}$ to $\mathbf{Z}_p^U$ and $\mathbf{Z}_p^D$, respectively, using the frequency components in $\mathbf{Y}_p^{U_1}$, $\mathbf{Y}_p^{U_2}$, $\mathbf{Y}_p^{D_1}$, and $\mathbf{Y}_p^{D_2}$, which are respectively expressed as

$$\begin{aligned} \mathbf{Z}_p^U &= \left[Z_p^U[0],\ Z_p^U[1],\ \cdots,\ Z_p^U[\frac{N_F}{2}-1] \right], \\ \mathbf{Z}_p^D &= \left[Z_p^D[0],\ Z_p^D[1],\ \cdots,\ Z_p^D[\frac{N_F}{2}-1] \right], \end{aligned} \quad (20)$$

where

$$\begin{aligned} Z_p^U[k] &= \begin{cases} |X_p^U[k]| & (k \notin \mathbf{K}_p^{U_3}) \\ 0 & otherwise, \end{cases} \\ Z_p^D[k] &= \begin{cases} |X_p^D[k]| & (k \notin \mathbf{K}_p^{D_3}) \\ 0 & otherwise. \end{cases} \end{aligned} \quad (21)$$

Using these reconstructed chirp signals, we can estimate the more accurate frequency shift by calculating the correlation between $Z_p^U[k]$ and $Z_p^D[k]$, which is expressed as

$$2\widehat{k}_e = \underset{q\in\{0,1,\cdots,2k_e^{MAX}\}}{\operatorname{argmax}} \sum_{k=0}^{\frac{N_F}{2}-1} Z_p^U[k] Z_p^D[k+q]. \quad (22)$$

In the same manner, the parameter in (19) can also be improved by using the signals that belong to $\mathbf{K}_p^{U_2}$ because the signals in $\mathbf{K}_p^{U_2}$ show the largest difference among the classified magnitude sets. Finally, an improved second recognition parameter $\widehat{\beta}_p$ is defined as

$$\widehat{\beta}_p = \frac{\sum_{k\in\mathbf{K}_p^{U_2}} \left(|X_p^U[k]|^2 - |\widehat{X}_p^U[k]|^2 \right)}{\sum_{k\in\mathbf{K}_p^{U_2}} |X_p^U[k]|^2}, \quad (23)$$

where $|\widehat{X}_p^U[k]|$ is expressed as

$$|\widehat{X}_p^U[k]| = \lceil |X_p^U[k]| - |X_p^D[k+2\widehat{k}_e]| \rceil_+. \quad (24)$$

If several reflectors that generate high-density clutter exist, α_p and $\widehat{\beta}_p$ show high values. Otherwise, both parameters have low values. Based on these, the high-density clutter environment recognition parameter can be defined by considering the two parameters, which is expressed as

$$G_p = \alpha_p \widehat{\beta}_p. \quad (25)$$

The proposed algorithm can recognize high-density clutter environments regardless of the velocity of the radar-equipped vehicle. In a particular case, such as a traffic congestion situation, if the number of vehicles having the same speed increases, α_p and $\widehat{\beta}_p$ can be increased. However, the probability that the speeds of nearby vehicles are completely identical and the corresponding f_{d_m} of that are the same is a very low in a real driving environment.

We tested the proposed algorithm for the test environments of Figs. 2 and 3, namely, Scenarios A and B, respectively. Figs. 5 (a) and (b) show $\lceil \mathbf{X}_p^U \rceil_{||}$ and $2\widehat{k}_e$-shifted $\lceil \mathbf{X}_p^D \rceil_{||}$ of Scenarios A and B, respectively. In both figures, the high-density clutter components have similar values. In particular, clutter components in Fig. 5 (b) show high similarities between $\lceil \mathbf{X}_p^U \rceil_{||}$ and $2\widehat{k}_e$-shifted $\lceil \mathbf{X}_p^D \rceil_{||}$ compared to those in Fig. 5 (a) because the tunnel environment of Scenario B is composed of a larger artificial road structure.

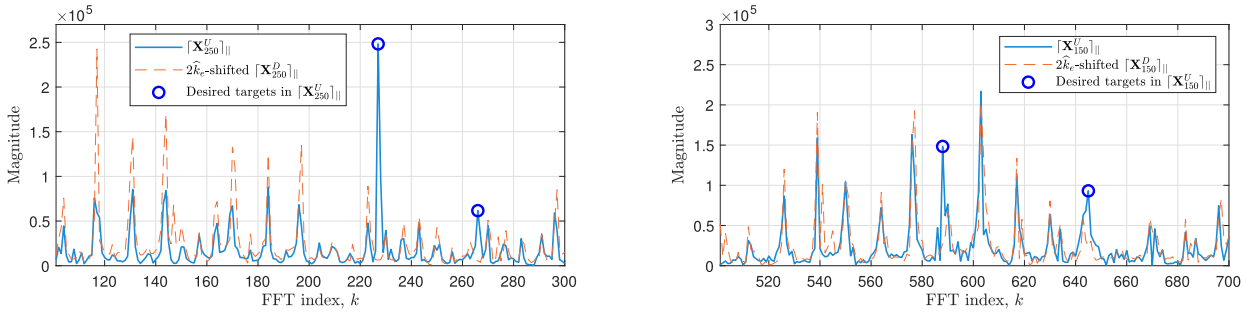

FIGURE 5. $\lceil \mathbf{X}_p^U \rceil_{||}$ and $2\widehat{k}_e$-shifted $\lceil \mathbf{X}_p^D \rceil_{||}$ (a) at $p = 250$ in Scenario A and (b) at $p = 150$ in Scenario B .

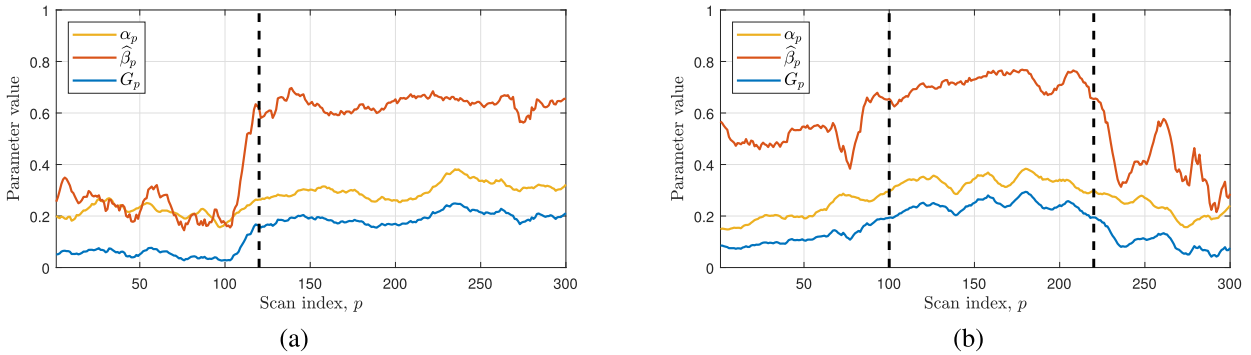

FIGURE 6. α_p, $\widehat{\beta}_p$, and G_p in (a) Scenario A and (b) Scenario B .

Figs. 6 (a) and (b) show the recognition results using the proposed recognition parameter for Scenarios A and B, respectively. The dashed line shown in Fig. 6 (a) denotes the starting point of the soundproof wall, and the dashed-line in Fig. 6 (b) denotes the starting and end points of the tunnel. N_1 is set to 20, because the number of target signals is limited to the scope of a few dozen [18]. Since the number of clutter signals is several times greater than N_1, we set N_2 to 100. To obtain reliable and stable recognition results, we applied a moving average filter. To avoid long output delays for present input values, the filter length is set to 5, which causes an output delay of 0.3 s. The delay time of 0.3 s does not significantly affect the recognition of the high-density clutter environments. For example, when the vehicle travels at a speed of 30.56 m/s (110 km/h), the vehicle can advance about 9.16 m. However, this is a short distance compared to the maximum detection distance (292 m) and does not cause a large difference in the time required to prepare for a high-density clutter environment in front of the travel path. In Fig. 6 (a), α_p, $\widehat{\beta}_p$, and G_p increase to high values when the radar-equipped vehicle enters the high-density clutter environment. In particular, $\widehat{\beta}_p$ responds more sensitively to the high-density environment than α_p. In Fig. 6 (b), α_p, $\widehat{\beta}_p$, and G_p increase to high values in the high-density clutter environment as in Fig. 6 (a). However, $\widehat{\beta}_p$ in Scenario B shows a higher value before entering and after exiting the high-density clutter environments. These high values are suppressed in the resultant G_p by multiplying $\widehat{\beta}_p$ by α_p. Thus, the effectiveness of α_p is confirmed in Scenario B. Finally, by determining a threshold value, we can recognize a high-density clutter environment. To determine the common threshold value, we tested various high-density clutter environments in the Republic of Korea. A threshold value of 0.15 showed the most stable results for the tested environments. Thus, we set the threshold value to 0.15.

To demonstrate the stability and effectiveness of our proposed algorithm, we also compare G_p with the recognition parameter using SE, which is proposed to recognize one of the common high-density clutter environments: the iron tunnel [8]. Figs. 7 (a) and (b) show the recognition results of our proposed method and the method in [8] for Scenarios A and B, respectively. The moving average filter was also applied with the same average length for the method in [8]. As shown in the figure, our proposed recognition parameter G_p exhibits more stable results in high-density clutter environments. For example, Fig. 7 (b) shows that when the radar-equipped vehicle drives through the tunnel, the recognition parameter that uses SE shows a large fluctuation compared to G_p. In addition, the SE parameter cannot clearly discriminate the high-density clutter environment because a larger value variation exists in the SE parameter. A comparison of the performance between β_p and $\widehat{\beta}_p$, $\alpha_p\beta_p$ is presented in Fig. 7. The recognition values using β_p are higher than those using $\widehat{\beta}_p$ in a normal road interval of both

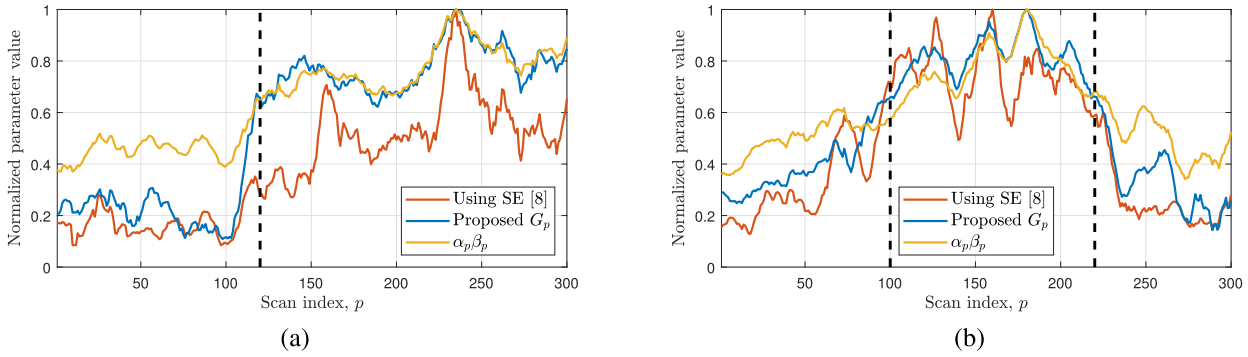

FIGURE 7. Recognition results of G_p and the parameter using Shannon entropy [8] in (a) Scenario A and (b) Scenario B.

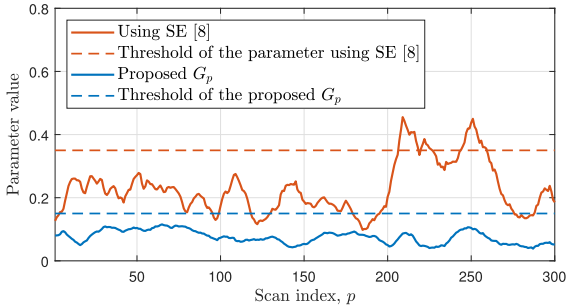

FIGURE 8. Recognition results of G_p and the parameter using Shannon entropy [8] in the normal environment in Fig. 1.

Scenarios. Under these circumstances, the ambiguity of the threshold settings and, correspondingly, the possibility of recognition errors, could increase. Therefore, small magnitude components that correspond to the elements in U_3 and D_3 should not be included in the calculation of $\widehat{\beta}_p$.

Fig. 8 shows the recognition results of our proposed method and that of the method in [8] for the normal environment shown in Fig. 1. The threshold value of the recognition parameter using SE is set to 0.35 as in [8]. These results are not normalized to compare the result for each threshold. Fig. 8 shows that the recognition parameter using SE misrecognizes the normal environment as a high-density clutter environment. However, our proposed algorithm guarantees stable recognition and does not misrecognize the driving environment.

In order to apply our proposed algorithm, the correlation between the components corresponding to $f_{b_m}^U$ and $f_{b_m}^D$ should be higher than the correlation between the components corresponding to $f_{b_l}^U$ and $f_{b_l}^D$. Even if a driving environment has a relatively small number of clutter signals, the proposed algorithm can be applied if the relationship between the correlation results is satisfied.

IV. PROPOSED HIGH-DENSITY CLUTTER SUPPRESSION METHOD

After the high-density clutter environment recognition, the high-density clutter signal should be suppressed to prevent degradation in the desired target detection performance. The high-density clutter in $\lceil \mathbf{X}_p^U \rceil_{||}$ can be suppressed by subtracting $2k_e$ shifted $\lceil \mathbf{X}_p^D \rceil_{||}$ from $\lceil \mathbf{X}_p^U \rceil_{||}$, because all M reflectors have the same frequency shift of $2k_e$ [17]. On the other hand, the beat frequencies of the L targets remain because they have different Doppler frequency shifts $2k_{d_l}$. In [17], $2\widetilde{k}_e$ in (17) is used as the amount of frequency shift, $2k_e$, for high-intensity clutter suppression. However, the noisy components corresponding to $\mathbf{K}_p^{U_3}$ and $\mathbf{K}_p^{D_3}$ lower the $2k_e$ estimation accuracy. For more reliable high-density clutter suppression, we used $2\widehat{k}_e$ in (22) as the estimated $2k_e$. Then, the high-density clutter suppressed up-chirp signal $\widehat{\mathbf{X}}_p^U$ is expressed as

$$\begin{aligned}\widehat{\mathbf{X}}_p^U &= \left[|X_p^U[0]|,\ |X_p^U[1]|,\ \cdots,\ |X_p^U[\frac{N_F}{2}-1-2\widehat{k}_e]|\right] \\ &\quad - \left[|X_p^D[2\widehat{k}_e]|,\ |X_p^D[2\widehat{k}_e+1]|,\ \cdots,\ |X_p^D[\frac{N_F}{2}-1]|\right] \\ &= \left[|\widehat{X}_p^U[0]|,\ |\widehat{X}_p^U[1]|,\ \cdots,\ |\widehat{X}_p^U[\frac{N_F}{2}-1-2\widehat{k}_e]|\right].\end{aligned} \tag{26}$$

As a result, the target detection performance can be improved using $\widehat{\mathbf{X}}_p^U$ instead of $\lceil \mathbf{X}_p^U \rceil_{||}$.

Fig. 9 shows the whole process of the proposed high-density clutter recognition and suppression for Scenarios A and B. Figs. 9 (a) and (b) show $\lceil \mathbf{X}_p^U \rceil_{||}$ for 300 scans. Then, using proposed parameter G_p, the high-density clutter environment is successfully recognized, as shown in Figs. 9 (c) and (d). After recognition, we apply our proposed clutter suppression method, and the results are shown in Figs. 9 (e) and (f). In addition, the suppression results for the 250-th and 150-th scans for each Scenario are shown in Figs. 9 (g) and (h). As shown in the figure, before the high-density clutter suppression, the signals from dense reflectors degrade the identification of the signals reflected from the desired targets; however, after the proposed clutter suppression, beat frequencies corresponding to the reflectors disappear and the beat frequencies corresponding to meaningful targets remain. Thus, improved target detection can be achieved by the CFAR algorithm when our proposed algorithm is used.

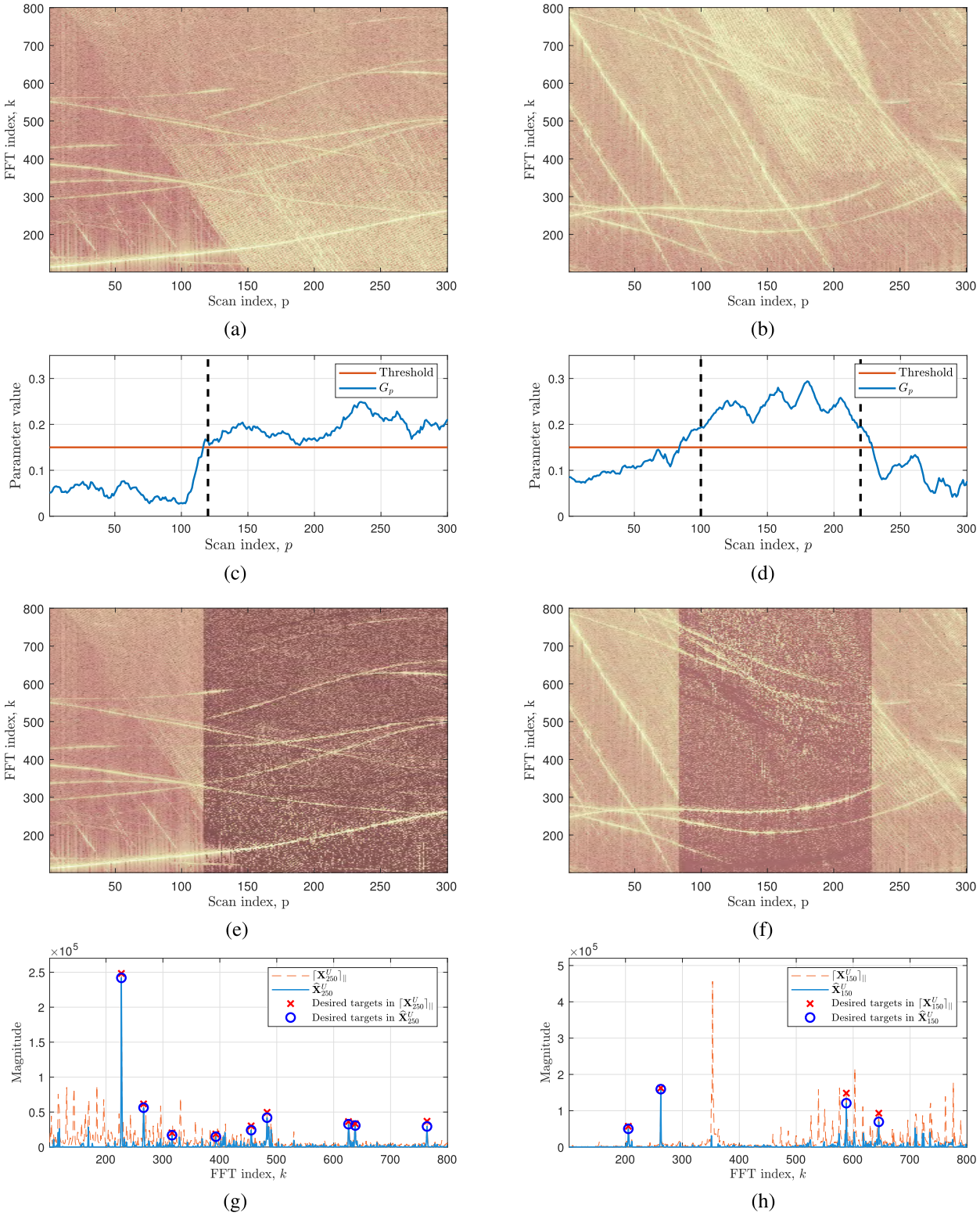

FIGURE 9. The whole process of the proposed high-density clutter recognition and suppression in Scenarios A and B .

V. CONCLUSION

In a high-density clutter environment such as tunnels and soundproof walls, many beat frequency components due to a number of reflectors are detected, which degrade the detection performance of automotive radars. Thus, we have proposed a recognition and suppression method for high-density

clutter environment in automotive FMCW radar systems. Using the different distributions of beat frequencies between the clutter environment and normal road environment, we proposed a recognition parameter for the clutter environment. In addition, the high-density clutter suppression using the correlation characteristics between the up-chirp and down-chirp received signals was also proposed. The proposed method was applied to the experimental results obtained from various road environments, and it showed that the high-density clutter was effectively recognized and suppressed using our proposed method. Therefore, enhanced target estimation from the clutter-suppressed signal was performed more stably, which can guarantee safety of drivers using automotive radar.

ACKNOWLEDGMENT

S. Lee was with Seoul National University (SNU), Seoul, South Korea.

REFERENCES

[1] G. Bresson, Z. Alsayed, L. Yu, and S. Glaser, "Simultaneous localization and mapping: A survey of current trends in autonomous driving," *IEEE Trans. Intell. Veh.*, vol. 2, no. 3, pp. 194–220, Sep. 2017.

[2] S. R. E. Datondji, Y. Dupuis, P. Subirats, and P. Vasseur, "A survey of vision-based traffic monitoring of road intersections," *IEEE Trans. Intell. Transp. Syst.*, vol. 17, no. 10, pp. 2681–2698, Oct. 2016.

[3] R. Thakur, "Scanning LIDAR in advanced driver assistance systems and beyond: Building a road map for next-generation LIDAR technology," *IEEE Consum. Electron. Mag.*, vol. 5, no. 3, pp. 48–54, Jul. 2016.

[4] K. Takagi, K. Morikawa, T. Ogawa, and M. Saburi, "Road environment recognition using on-vehicle LIDAR," in *Proc. IEEE Intell. Vehicles Symp.*, Jun. 2006, pp. 120–125.

[5] M. I. Skolnik, *Introduction to Radar Systems*, 3rd ed. New York, NY, USA: McGraw-Hill, 2001.

[6] M. Schneider, "Automotive radar—Status and trends," in *Proc. IEEE German Microw. Conf. (GeMiC)*, Apr. 2005, pp. 144–147.

[7] J.-E. Lee, H.-S. Lim, S.-H. Jeong, S.-C. Kim, Y.-S. Choi, and H.-C. Shin, "Enhanced iron-tunnel recognition for automotive radars," in *Proc. 16th Int. Radar Symp. (IRS)*, Jun. 2015, pp. 149–154.

[8] J.-E. Lee, H.-S. Lim, S.-H. Jeong, S.-C. Kim, and H.-C. Shin, "Enhanced iron-tunnel recognition for automotive radars," *IEEE Trans. Veh. Technol.*, vol. 65, no. 6, pp. 4412–4418, Jun. 2016.

[9] C. Lundquist, U. Orguner, and T. B. Schon, "Tracking stationary extended objects for road mapping using radar measurements," in *Proc. IEEE Intell. Vehicles Symp.*, Jun. 2009, pp. 405–410.

[10] F. Diewald, J. Klappstein, F. Sarholz, J. Dickmann, and K. Dietmayer, "Radar-interference-based bridge identification for collision avoidance systems," in *Proc. IEEE Intell. Vehicles Symp.*, Jun. 2011, pp. 113–118.

[11] F. Janda, S. Pangerl, E. Lang, and E. Fuchs, "Road boundary detection for run-off road prevention based on the fusion of video and radar," in *Proc. IEEE Intell. Vehicles Symp.*, Jun. 2013, pp. 1173–1178.

[12] J.-E. Lee, H.-S. Lim, S.-H. Jeong, H.-C. Shin, S.-W. Lee, and S.-C. Kim, "Harmonic clutter recognition and suppression for automotive radar sensors," *Int. J. Distrib. Sensor Netw.*, vol. 13, no. 9, pp. 1–11, Sep. 2017.

[13] E. Hyun, W. Oh, and J.-H. Lee, "Multi-target detection algorithm for FMCW radar," in *Proc. IEEE Radar Conf.*, May 2012, pp. 338–341.

[14] T. M. Cover and J. A. Thomas, *Elements of Information Theory*, 2nd ed. Hoboken, NJ, USA: Wiley, 2006.

[15] H.-B. Lee, J.-E. Lee, H.-S. Lim, S.-H. Jeong, and S.-C. Kim, "Clutter suppression method of iron tunnel using cepstral analysis for automotive radars," *IEICE Trans. Commun.*, vol. E100-B, no. 2, pp. 400–406, Feb. 2017.

[16] S. Lee, Y.-J. Yoon, J. Yoon, H. Sim, and S.-C. Kim, "Periodic clutter suppression in iron road structures for automotive radar systems," *IET Radar, Sonar Navigat.*, vol. 12, no. 10, pp. 1146–1153, Sep. 2018.

[17] J. Yoon, S. Lee, and S.-C. Kim, "Enhanced target detection in high-intensity clutter environments for automotive radar systems," in *Proc. 19th IEEE Int. Radar Symp. (IRS)*, Jun. 2018, pp. 1–9.

[18] Y. Okamoto, I. Matsunami, and A. Kajiwara, "Moving vehicle discrimination using Hough transformation," in *Proc. IEEE Radio Wireless Symp. (RWS)*, Jan. 2011, pp. 367–370.

[19] B. R. Mahafza, *Radar Systems Analysis and Design Using MATLAB*. Boca Raton, FL, USA: CRC Press, 2000.

[20] A. G. Stove, "Linear FMCW radar techniques," *IEE Proc. F-Radar Signal Process.*, vol. 139, no. 5, pp. 343–350, Oct. 1992.

[21] S. M. Patole, M. Torlak, D. Wang, and M. Ali, "Automotive radars: A review of signal processing techniques," *IEEE Signal Process. Mag.*, vol. 34, no. 2, pp. 22–35, Mar. 2017.

[22] H. Rohling, "Radar CFAR thresholding in clutter and multiple target situations," *IEEE Trans. Aerosp. Electron. Syst.*, vol. AES-19, no. 4, pp. 608–621, Jul. 1983.

[23] L. Stanislas and T. Peynot, "Characterisation of the delphi electronically scanning radar for robotics applications," in *Proc. Australas. Conf. Robot. Autom.*, Dec. 2015, pp. 2–4.

JUNGMIN YOON received the B.S. degree in electrical and electronic engineering from Yonsei University, Seoul, South Korea, in 2009, and the M.S. degree in electrical and computer engineering from Seoul National University, Seoul, in 2011, where he is currently pursuing the Ph.D. degree, as a member of the Samsung Fellowship Program. Since 2011, he has been with Samsung Electronics Co., Ltd., Suwon, South Korea. He has contributed to the development of next-generation wireless communication systems. His current interests include the research and development of millimeter-wave wireless communication systems and millimeter-wave radar systems.

SEONGWOOK LEE received the B.S. and Ph.D. degrees in electrical and computer engineering from Seoul National University (SNU), Seoul, South Korea, in 2013 and 2018, respectively. Since 2018, he has been a Staff Researcher with the Samsung Advanced Institute of Technology (SAIT), Suwon, South Korea. He has published more than 30 papers in radar signal processing. His current research interests include automotive radar signal processing techniques, such as improved angle estimation, target recognition and classification, clutter suppression, and mutual interference mitigation. He received the Distinguished Ph.D. Dissertation Award from the Department of Electrical and Computer Engineering, SNU. He is a Reviewer of international journals, such as *Ad Hoc Networks* (Elsevier), *ICT Express* (Elsevier), the IEEE Access, the IEEE Communications Letters, the IEEE Sensors Journal, the IEEE Systems Journal, the IEEE Transactions on Intelligent Transportation Systems, the IEEE Transactions on Signal Processing, *IET Radar, Sonar & Navigation*, *MDPI Algorithms*, and *MDPI Sensors*.

SOHEE LIM received the B.S. degree in electrical and computer engineering from Seoul National University, Seoul, South Korea, in 2017, where she is currently pursuing the M.S. degree. Her current research interest includes radar signal processing techniques, particularly on clutter and interference suppression.

SEONG-CHEOL KIM received the B.S. and M.S. degrees from Seoul National University, Seoul, South Korea, in 1984 and 1987, respectively, and the Ph.D. degree from the Polytechnic Institute of NYU, Brooklyn, NY, USA, in 1995, all in electrical engineering. From 1995 to 1999, he was with the Wireless Communications Systems Engineering Department, AT&T Bell Laboratories, Holmdel, NJ, USA. Since 1999, he has been a Professor with the Department of Electrical and Computer Engineering, Seoul National University. His current research interests include system engineering of wireless communications including millimeter-wave channel modeling, localization algorithms, power-line communications, and automotive radar signal processing.